### CHEMICAL PHYSICS

# Improving SABRE hyperpolarization with highly nonintuitive pulse sequences: Moving beyond avoided crossings to describe dynamics

Shannon L. Eriksson<sup>1,2</sup>\*, Jacob R. Lindale<sup>1</sup>, Xiaoqing Li<sup>3</sup>, Warren S. Warren<sup>1,2,3,4</sup>\*

Signal amplification by reversible exchange (SABRE) creates "hyperpolarization" (large spin magnetization) using a transition metal catalyst and parahydrogen, addressing the sensitivity limitations of magnetic resonance. SABRE and its heteronuclear variant X-SABRE are simple, fast, and general, but to date have not produced polarization levels as large as more established methods. We show here that the commonly used theoretical framework for these applications, which focuses on avoided crossings (also called level anticrossings or LACs), steer current SABRE and X-SABRE experiments away from optimal solutions. Accurate simulations show astonishingly rich and unexpected dynamics in SABRE/X-SABRE, which we explain with a combination of perturbation theory and average Hamiltonian approaches. This theoretical picture predicts simple pulse sequences with field values far from LACs (both instantaneously and on average) using different terms in the effective Hamiltonian to strategically control evolution and improve polarization transfer. Substantial signal enhancements under such highly nonintuitive conditions are verified experimentally.

Copyright © 2022
The Authors, some rights reserved; exclusive licensee
American Association for the Advancement of Science. No claim to original U.S. Government Works. Distributed under a Creative
Commons Attribution
NonCommercial
License 4.0 (CC BY-NC).

### INTRODUCTION

Nuclear magnetic resonance (NMR) techniques have wide applications in chemistry, physics, materials science, and medicine. Unfortunately, because the interaction of nuclei with an external magnetic field only induces small energy differences between spin states, the sensitivity of these techniques is fundamentally limited. Hyperpolarization methods artificially alter spin populations to induce polarizations far beyond thermal equilibrium by transferring polarization from a source of spin order to the target nucleus. Techniques such as dissolution dynamic nuclear polarization (DNP) (1) and spin exchange optical pumping (SEOP) (2) have been in use for decades and have matured to the point of clinical applicability but are limited by expense and need for specialized personnel to operate equipment. An alternative method, originally introduced as signal amplification by reversible exchange (SABRE) (3, 4), enables large signal enhancements in many different molecules at a small fraction of the cost of other techniques. Multiple variants have more recently been demonstrated under high-field and low-field conditions (5–13), some of which can directly produce longer-lived heteronuclear polarization (these variants are called X-SABRE here). SABRE and the variants are much faster, simpler, and less expensive than DNP or SEOP; hundreds of different molecules have been successfully polarized (14); and the methods, in principle, should be scalable to large quantities. However, to date, the total achievable polarization at one time has been lower than in DNP or SEOP. Here, we show that a notable factor in this limitation is that the accepted method for visualizing SABRE effects, which focuses on avoided crossings (also called level anticrossings or LACs), steers current experiments away from optimal solutions. We propose and experimentally demonstrated sequences that are quite nonintuitive from the LAC perspective, demonstrate substantial signal enhancements, and develop a different framework to better guide intuition for pulse sequence design.

SABRE derives spin order from parahydrogen, the singlet state  $[1/\sqrt{2}(|\alpha\beta\rangle-|\beta\alpha\rangle)]$  of the hydrogen molecule, using reversible interactions between a polarization transfer catalyst (PTC), a parahydrogen, and a target ligand (Fig. 1). The parahydrogen creates a singlet hydride pair bound reversibly to the Ir coordination center, typically exchanging with rates  $k_{\rm H}\approx 1$  to  $5~{\rm s}^{-1}$ . A target ligand, such as  $^{15}{\rm N}$ -acetonitrile in this example, also reversibly binds to the complex, typically with a rate  $k_{\rm L}\approx 5$  to  $50~{\rm s}^{-1}$  (12,15-17). Coligands, like the unlabeled  $^{14}{\rm N}$ -pyridine shown in Fig. 1, are sometimes used to modify exchange rates for the target ligand to more optimal values (18). Under certain magnetic field conditions, scalar couplings between the hydrides and nuclei in the bound target ligand(s) facilitate spin order transfer into bulk magnetization on the target.

Polarization transfer in SABRE experiments has been generally explained as resonant population transfer at an avoided crossing or LAC (5, 10, 19, 20). Avoided crossings provide a powerful framework in many spectroscopic applications, going back nearly a century. In a two-level system, where the states are connected by some coupling, the eigenstates of the system become strongly mixed when the energies of the states become equivalent (21–27). Thus, for example, adiabatic passage is commonly treated in an avoided crossing picture and can enable quantitative state-to-state transfer. Because SABRE hyperpolarization operates by passing population out of some overpopulated initial state (with singlet order hydrides) into a desired final state with magnetization on the target nucleus, viewing this process as reflecting LAC dynamics seems reasonable. For this reason, essentially all SABRE variants used the LAC approximation of polarization transfer for design and optimization.

This discussion will focus on the low-field SABRE variants, where strong coupling between the hydrides and target nucleus is exploited to couple our initial and target spin states. Proton-only SABRE approaches a LAC matching condition when the chemical shift difference between the hydrides and target <sup>1</sup>H nucleus is on the order

<sup>&</sup>lt;sup>1</sup>Department of Chemistry, Duke University, Durham, NC 27708, USA. <sup>2</sup>School of Medicine, Duke University, Durham, NC 27708, USA. <sup>3</sup>Department of Physics, Duke University, Durham, NC 27708, USA. <sup>4</sup>Department of Physics, Chemistry, Biomedical Engineering, and Radiology, Duke University, Durham, NC 27704, USA.

<sup>\*</sup>Corresponding author. Email: shannon.eriksson@duke.edu (S.L.E.); wwarren@duke.edu (W.S.W.)

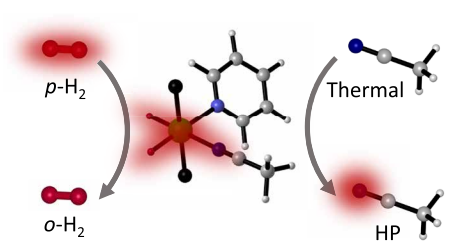


**Fig. 1. Exchange interactions in SABRE with an Ir(IMes) catalyst.** Parahydrogen, a target ligand ( $^{15}$ N-acetonitrile), and a stabilizing coligand ( $^{14}$ N-pyridine) exchange at the equatorial sites to form transient spin coupling networks for polarization transfer (46). The example system shown here is  $Ir(H)_2(IMes)(pyr)_2(^{15}N-acetonitrile)$  with inactive ligands in the axial positions omitted for clarity.

of the scalar couplings in the spin system (around 6.5 mT) (3–5). Heteronuclear X-SABRE techniques have expanded the polarizable nuclear targets to include heteronuclei such as  $^{15}$ N,  $^{13}$ C,  $^{19}$ F, and  $^{31}$ P (6, 28–31). In that case, the origin of the resonance frequency difference between the hydrides and target nucleus is the difference in gyromagnetic ratios, not chemical shifts, and this implies a much smaller magnetic field ( $\sim$  $\mu$ T) to establish this matching condition (32). Figure 2 shows a simple example, an X-SABRE experiment where continuous application of a very small magnetic field B results in substantial signal enhancement.

While LACs have proved to be useful in designing these initial experiments, SABRE presents a system with stochastic modulation from exchange and dissipation from relaxation acting on the same time scale as the coherent dynamics. There is no a priori theoretical justification for assuming avoided crossings give the optimum field. More sophisticated theoretical models have been developed to quantitatively describe polarization transfer in SABRE in the setting of chemical exchange (17, 33–36). While these models can be useful in optimization of experimental parameters under known experimental protocols, they lack intuitive utility as guides for constructing new experiments. Here, we first demonstrate that SABRE/X-SABRE experiments built around LAC matching conditions often lead to suboptimal polarization transfer conditions. We then show that pulse sequences, which stray far from LAC resonance conditions (both instantaneously and on average), yield large enhancements experimentally.

One example is shown in Fig. 3. At zero field, simple symmetry arguments imply that no magnetization is ever created. A field of -22.35 μT (approaching Earth's magnetic field) is about three orders of magnitude away from the LAC condition, so again, no magnetization is produced. Yet, Fig. 3 demonstrates that pulse sequences combining these field conditions can result in substantial signal enhancements. Figure 3A demonstrates sharp features indicating magnetization enhancement in pulse sequences where the field never approaches the LAC condition transiently or on average. On the left side of Fig. 3, the white dotted line corresponds to an average magnetic field at the experimental optimum in Fig. 2. However, all of the features at higher field are unexpected, as they have no relationship to the LAC condition. The black lines correspond to combinations of field pulse areas where the precession difference between the hydride and ligand spins is an integral number of cycles  $(\theta = 2\pi B_d \tau_d (\gamma_H - \gamma_N) = 2\pi n)$ . Signal increases with larger pulse area, and Fig. 3C shows an example of a much larger pulse area that yields about a factor of three enhancement.

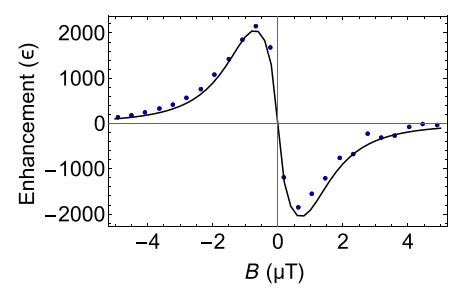


**Fig. 2. X-SABRE magnetic field profile.** The final signal enhancement for  $^{15}$ N-acetonitrile in an  $Ir(H)_2(IMes)(pyr)_2(^{15}$ N-acetonitrile) PTC with continuous application of a magnetic field B. Black line shows theoretical simulation of a  $Ir(H)_2(IMes)(pyr)_2(^{15}$ N-acetonitrile) system  $(k_L = 20 \text{ s}^{-1}, k_H = 2 \text{ s}^{-1}, [\text{catalyst}]: [ligand] = 1:20, and 30-s evolution). Data points show experimental enhancement relative to thermal magnetization measured at 1 T [sample composition: 5 mM Ir(IMes), 50 mM <math>^{14}$ N-pyridine, and 100 mM  $^{15}$ N-acetonitrile in CD<sub>3</sub>OD].

We will use a combination of average Hamiltonian theory and perturbation theory to expand our conceptual understanding of the dynamics, explain the nonintuitive structure in calculations such as Fig. 3, and predict the features necessary to guide optimization of SABRE/X-SABRE. This allows us to derive and demonstrate simple motifs, which give large signal enhancements and are robust to experimental imperfections, such as field inhomogeneity. More generally, we show that multiple fundamental limitations in polarization transfer are addressed simply by what we call two-state SABRE: Two different time periods with different effective Hamiltonians can provide substantial improvements. Such sequences are easy to implement and improve the robustness of the SABRE/X-SABRE effect, particularly in the very slow and very fast exchange limits.

### **RESULTS**

### Theoretical perspectives on SABRE dynamics

We begin by briefly reviewing the traditional theoretical framework, focusing here on two simple but illustrative cases used widely in SABRE: the three-spin case with a single target ligand nucleus  $\hat{L}$  and the four-spin case with two target ligands  $\hat{L}_1$  and  $\hat{L}_2$ . The target  $\hat{L}$  is  $^1\text{H}$  in SABRE and commonly  $^{15}\text{N}$  in X-SABRE variants such as SABRE in Shield Enables Alignment Transfer to Heteronuclei (SABRE-SHEATH). In both spin systems, two hydride spins  $\hat{I}_1$  and  $\hat{I}_2$  with singlet order population  $S_{\text{H}} = (|\alpha_1 \beta_2\rangle - |\beta_1 \alpha_2\rangle)/\sqrt{2}$  derived from binding parahydrogen are bound to the central iridium atom, and  $\alpha_n$  and  $\beta_n$  are the spin-up and spin-down states of hydride spin n; the other three hydrogen states are  $|T_{1,\,\text{H}}\rangle = |\alpha_1\alpha_2\rangle, |T_{0,\text{H}}\rangle = (|\alpha_1 \beta_2\rangle + |\beta_1 \alpha_2\rangle)/\sqrt{2}$ , and  $|T_{-1,\,\text{H}}\rangle = |\beta_1\beta_2\rangle$ .

In the three-spin case, the ligand initially has thermally distributed populations of 50% spin up ( $|\alpha_L\rangle$ ) and 50% spin down ( $|\beta_L\rangle$ ). When parahydrogen and the target nucleus transiently associate with the iridium catalyst, these states are combined to give an initial density matrix of 50%  $|S_H\alpha_L\rangle$  and 50%  $|S_H\beta_L\rangle$ . This can be written as

$$\hat{\rho}_0 = \left(\frac{1}{4}\hat{1}_4 - \hat{I}_1 \cdot \hat{I}_2\right) \otimes \frac{1}{2}\hat{1}_2 \tag{1}$$

The matrices  $\hat{1}_q$  are the identity matrices of dimension  $q \times q$ . It is often an excellent approximation to assume that the ligand is only coupled to one of the two hydrides (here chosen as spin 1). The evolution of these states in an externally applied magnetic field is

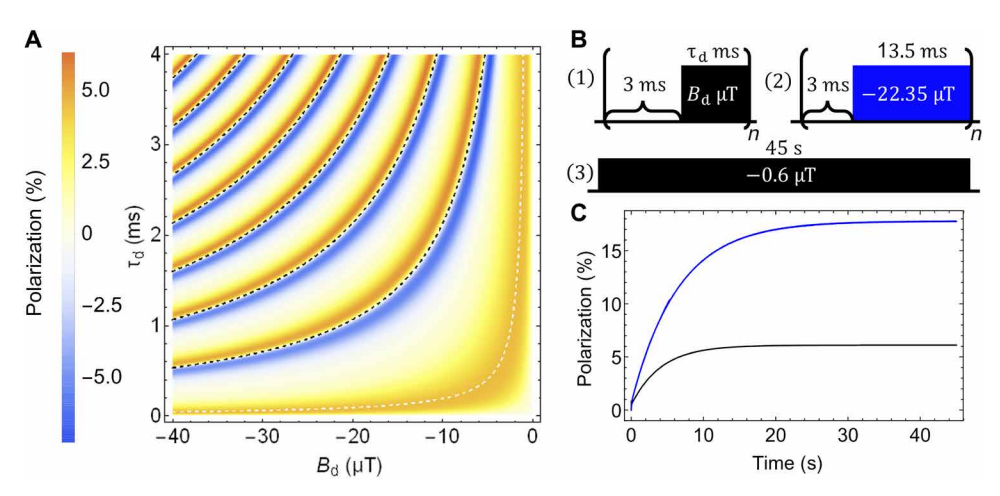


Fig. 3. Effects of several simple sequences (top right) on X-SABRE magnetization production. (A) Polarization after application of pulse sequence 1 on an Ir(H)<sub>2</sub>(IMes) (pyr)<sub>2</sub>( $^{15}$ N-acetonitrile) system ( $k_L = 20 \text{ s}^{-1}$ ,  $k_H = 2 \text{ s}^{-1}$ , [catalyst]: [ligand] = 1 : 20, and hydride and all acetonitrile spins included). The white dashed line shows a local maximum, with an average field of  $-0.6 \,\mu\text{T}$  close to the optimum continuous field condition. Black dashed lines mark pulse conditions where  $\theta = 2\pi B_d \tau_d (\gamma_H - \gamma_N) = 2\pi n$ . The positive and negative bands around these contour lines are unexpected in the normal picture and correspond to increased magnetization. (B) Pulse sequences used to generate numerical simulation results for (A) and (C). (C) Polarization buildup over time under sequence 2 (blue) yields a threefold increase in polarization over evolution under the optimal continuous field [sequence 3 in (B)] shown in black.

governed by the nuclear spin Hamiltonian  $(\widehat{\mathcal{H}})$  shown, here in natural units  $(\hbar = 1)$ 

$$\widehat{\mathcal{H}}' = \omega_{H}(\hat{I}_{1z} + \hat{I}_{2z}) + \omega_{L}\hat{L}_{z} + 2\pi J_{HH}\hat{I}_{1} \cdot \hat{I}_{2} + 2\pi J_{HL}\hat{I}_{1} \cdot \hat{L}$$
 (2)

The Zeeman terms  $[\omega_H(\hat{I}_{1z} + \hat{I}_{2z}) + \omega_L \hat{L}_z]$  define the evolution of individual spins in the magnetic field (*B*) with the Larmor frequencies  $\omega_n = -\gamma_n B$ . It is useful to write this Hamiltonian in a slightly different form

$$\widehat{\mathcal{H}}' = \omega_{H}(\hat{I}_{1z} + \hat{I}_{2z} + \hat{L}_{z}) + 2\pi J_{HH} \hat{I}_{1} \cdot \hat{I}_{2} + 2\pi J_{HL} \hat{I}_{1z} \hat{L}_{z} - (\omega_{H} - \omega_{L}) \hat{L}_{z} + 2\pi J_{HL} (\hat{I}_{1x} \hat{L}_{x} + \hat{I}_{1y} \hat{L}_{y})$$
(3)

The first term, proportional to the z component of the total angular momentum, commutes with the rest of the Hamiltonian. Thus, the couplings do not create net z angular momentum, but they can create opposite-sign angular momentum components on the hydrogen and ligands. As an aside, this implies that SABRE evolution never creates net magnetization either, because the gyromagnetic ratios of I and L are the same. The created ligand magnetization is counterbalanced by orthohydrogen-reversed magnetization, which then bubbles away or relaxes quickly. X-SABRE experiments do create net magnetization because the gyromagnetic ratios of I and L are different.

We are ultimately interested in optimizing  $\hat{L}_z$ , the magnetization on the ligands, which survives dissociation of the ligand complex. This also commutes with the first term in Eq. 3. It is then trivial to show that this term has no effect of the production of magnetization, so we ignore it in what follows, writing

$$\widehat{\mathcal{H}}' = 2\pi J_{\text{HH}} \hat{I}_{1} \cdot \hat{I}_{2} + 2\pi J_{\text{HL}} \hat{I}_{1z} \hat{\mathcal{L}}_{z} - \Delta \omega_{\text{HL}} \hat{\mathcal{L}}_{z} + 2\pi J_{\text{HL}} (\hat{I}_{1x} \hat{\mathcal{L}}_{x} + \hat{I}_{1y} \hat{\mathcal{L}}_{y})$$
(4)

where the difference  $\Delta\omega_{HL}=\omega_{H}-\omega_{L}$  is commonly >20 parts per million in SABRE (from chemical shift differences between protons), but  $\Delta\omega_{HL}\approx 1.1\omega_{H}$  in SABRE-SHEATH with  $^{15}N$  (since  $\gamma_{N}\approx -\gamma_{H}/10$ ).

The one parameter under the control of the experimenter is  $\Delta\omega_{HL}$  in the third term, which commutes with all but the last term in Eq. 4.

The extremely simple expression in Eq. 4 is powerful for providing physical insight. We start by looking at the traditional, continuous field SABRE/X-SABRE case. The LAC condition is at fields where the overpopulated  $|S_{H}\alpha_{L}\rangle$  state and empty  $|T_{1,H}\beta_{L}\rangle$  state have nearly diagonal elements, and the coupling mixes the two states. One  $3\times3$  block matrix is shown below; the rest are written out in the Supplementary Materials

$$\langle T_{1,H} \beta_{L} \rangle \mid T_{0,H} \alpha_{L} \rangle \mid S_{H} \alpha_{L} \rangle$$

$$\langle T_{1,H} \beta_{L} \mid$$

$$\langle T_{0,H} \alpha_{L} \mid$$

$$\langle S_{H} \alpha_{L} \mid$$

$$\langle S_{H} \alpha_{L} \mid$$

$$\begin{pmatrix} \alpha_{H} - \omega_{L} & \frac{\pi J_{HL}}{\sqrt{2}} & \frac{\pi J_{HL}}{\sqrt{2}} \\ \frac{\pi J_{HL}}{\sqrt{2}} & \frac{\pi J_{HL}}{2} & -\frac{\pi J_{HL}}{2} \\ \frac{\pi J_{HL}}{\sqrt{2}} & -\frac{\pi J_{HL}}{2} & -2\pi J_{HH} + \frac{\pi J_{HL}}{2} \end{pmatrix}$$

$$(5)$$

The diagonal elements for  $|S_H\alpha_L\rangle$  and  $|T_{1,\,H}\beta_L\rangle$  are equal when  $\Delta\omega_{HL}=-2\pi J_{HH}+\pi J_{HL}/2$ . In SABRE (with a proton target), the hydride and target nuclei are separated by four or more bonds, giving a smaller  $J_{HL}\approx 1$  Hz and  $\Delta\omega_{HL}\approx -2\pi J_{HH}$  matching condition. In the early SABRE papers (3, 33),  $J_{HH}$  was assumed to be positive and about +8 Hz. Common chemical shift differences between target and hydride protons indicate a LAC condition around 6.5 mT, and efficient polarization transfer was achieved at around this field. The first X-SABRE papers (6, 7) demonstrated polarization buildup around  $\pm 0.5 \, \mu T$ . A typical coupling  $J_{HL}\approx -20$  Hz corresponds to a LAC matching condition at  $-0.4 \, \mu T$ , consistent with Fig. 2 and initial SABRE-SHEATH experimental evidence.

Another LAC is found at positive magnetic field when  $\Delta\omega_{\rm HL}=2\pi J_{\rm HH}-\pi J_{\rm HL}/2$ , now between the  $|S_{\rm H}\beta_{\rm L}\rangle$  state and  $|T_{-1,\,{\rm H}}\alpha_{\rm L}\rangle$  state, which would create opposite-sign magnetization on the ligands. This is the basic approach behind the design of essentially all low-field SABRE and X-SABRE experiments. Approximating  $|S_{\rm H}\alpha_{\rm L}\rangle$  and  $|T_{1,\,{\rm H}}\beta_{\rm L}\rangle$  as a two-level system leads, for example, to the coherently pumped SABRE idea that the population can oscillate back

and forth only when the diagonal elements are nearly matched, and thus, interrupting the evolution by switching to high field at a maximum can give improved polarization (12).

A similar calculation for the four-level system (in the Supplementary Materials) gives a 4 × 4 matrix and two 2 × 2 matrices where the ligand-hydride coupling can create ligand magnetization. The states  $|S_HS_L\rangle$  and  $|T_{1,H}T_{-1,L}\rangle$  have the same diagonal values when  $\Delta\omega_{HL} = -2\pi(J_{HH} + J_{LL}) + \pi J_{HL}$ . In addition, the states  $|S_HT_{1,L}\rangle$  and  $|T_{1,H}S_L\rangle$  have the same diagonal values when  $\Delta\omega_{HL} = -2\pi(J_{HH} - J_{LL})$ . Both of these cases create net spin-down magnetization on the ligand nucleus at negative fields. Parallel arguments apply to the two corresponding LACs at positive field, which create positive magnetization.

Of course, reducing a complex quantum mechanical system to this extent is an oversimplification, which is made worse when there are multiple couplings. In the X-SABRE case,  $I_{\rm HL}$  often exceeds  $I_{\rm HH}$ , which couples in states other than the initial and target states (for example,  $|T_{0,H}\alpha_L\rangle$  in Eq. 5). In addition, the catalyst dynamics is exceedingly complex, as exchange rates (both of the ligands and of the parahydrogen), internal couplings, and resonance frequency differences are all very similar. Still, the commonly explored cases tend to look like in Fig. 2, with similar peak fields. A subtle point is that later papers showed clearly that  $J_{\rm HH}$  is negative (37–40). This has a consequence that seems to have been unappreciated by the community: It markedly changes the LAC condition. For example, for the <sup>15</sup>N-acetonitrile system ( $J_{NH} = -25.41$  Hz and  $J_{HH} = -8$  Hz), the LAC occurs at  $B = \pm 0.04 \,\mu\text{T}$ , an order of magnitude below the actual experimental maximum in Fig. 2. Since there are multiple coupled levels in Eq. 4 (or in the four-spin system), the predicted LAC depends somewhat on the basis set (41), but none of these choices (or an exact diagonalization, as done in the Supplementary Materials) substantially improve the fit. Thus, there is actually a

large amount of experimental evidence that something is considerably off with the LAC perspective.

We have recently developed a new numerical modeling approach for exchanging systems, which is extremely useful in the practical limits commonly seen in SABRE (17). These simulation methods handle exchange to infinite order in perturbation theory, making it feasible to take large time steps in the spin evolution without compromising accuracy. This technique has already shown robust agreement with experimental results. This, in turn, lets us explore a wider range of conditions than is easily accessible experimentally and is again shown here to be directly validated by targeted experiments. We start by looking at various conditions in standard continuous field SABRE and X-SABRE (Fig. 4) to show an unexpected result: Except under specific exchange regimes, the LAC matching condition does not predict maximum polarization transfer, and the optimal conditions are a very strong function of exchange rate (which never appears in the LAC calculation). The curves look quite similar in the three- and four-spin models (in the Supplementary Materials) and even in more complex systems.

The LAC prediction is largely accurate only for slow exchange rates and small  $J_{HL}$ . For exchange in the range that is commonly encountered experimentally, and particularly for the large couplings commonly found in X-SABRE, the optimum field far exceeds the LAC prediction. Thus, low experimental enhancements on rapidly exchanging systems can be partially attributed to the utilization of an optimal field found at a lower exchange rate. It has been demonstrated experimentally that the optimal continuous field is dependent on temperature (32).

Figure 4 also shows that common heteronuclear couplings in X-SABRE ( $\approx$ 20 Hz) are far larger than the optimum for creating polarization. Figure 4 would look identical for SABRE, with a rescaling of the y axis by about 30,000 (the dotted line would be at

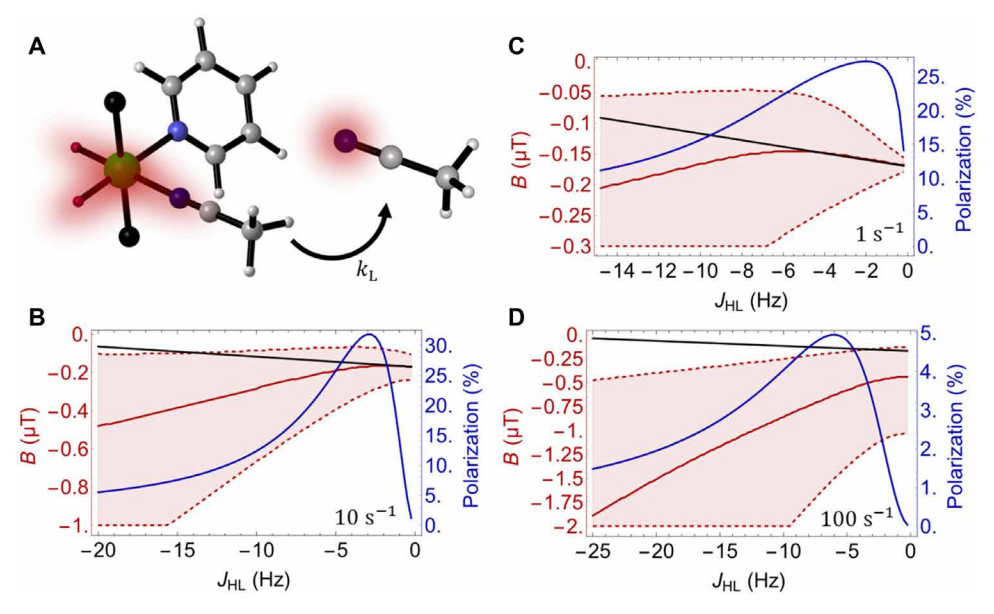


**Fig. 4. Discrepancies between optimal polarization transfer fields and LAC matching conditions in continuous field calculations.** (**A**) Truncated AA'X spin system with incorporated spins highlighted in red. (**B**) The field condition where maximum polarization transfer occurs is shown in red with dashed lines showing where 50% optimal polarization transfer occurs. Polarization at the optimal field condition is shown in blue after 10 s of exposure to magnetic field  $B_p$  with variable  $J_{HL}$  couplings for  $k_L = 1 \text{ s}^{-1}$ , (**C**)  $k_L = 10 \text{ s}^{-1}$ , and (**D**)  $k_L = 100 \text{ s}^{-1}$ . Black lines correspond to the AA'X LAC condition  $2\pi B_p(\gamma_H - \gamma_N) = 2\pi J_{HH} - \pi J_{HL}/2$ . Additional simulation parameters: [catalyst]: [ligand] = 1:20 and  $k_H = 1 \text{ s}^{-1}$ .

 $B_{\rm d}=6.5~{\rm mT}$  for  $J_{\rm HH}=0~{\rm Hz}$ ), which implies that normal SABRE couplings ( $\approx 1~{\rm Hz}$ ) are smaller than optimal except for very slow exchange.

Figure 5 shows coherently pumped SABRE, which uses two alternating field conditions to transser polarization more efficiently in the setting of chemical exchange. The evolution field presumably brings the system to the LAC condition where the off-diagonal matrix elements in Eq. 5 pump magnetization in and out of the ligand, with an oscillation frequency of  $J_{\rm HL}/\sqrt{2}$  (hence an expected maximum at  $\tau_p = 1/(\sqrt{2} J_{HL})$ . Then an off-resonant field condition halts polarization transfer by bringing the field away from the LAC matching condition and allowing chemical exchange to "replenish" the polarization transfer complex. Coherently pumped SABRE-SHEATH pulse sequences use the LAC-based description of polarization transfer in SABRE to produce the most efficient transfer (in a two-level approximation). However, use of the LAC matching condition is only optimal for a very limited set of exchange rates. For rapid exchange in particular, using the LAC condition leads to substantial signal attenuation. Again, larger spin systems (in the Supplementary Materials) provide very similar results.

Figures 4 and 5 clearly demonstrate that the LAC approach often leads to flawed prediction in foundational SABRE and X-SABRE experiments. We will now propose a different strategy for understanding polarization dynamics in SABRE experiments that will provide intuitive justification for the construction of pulse sequences outside of the LAC framework. Evolution of the density matrix  $\hat{\rho}$  under the nuclear spin Hamiltonian is dictated by the Liouville–von Neumann equation  $\partial \hat{\rho}/\partial t = i \, [\, \hat{\rho}, \widehat{\mathcal{H}} \,]$ . Using a Taylor series expansion of the solution of this differential equation, we can separate out the time dependence for the generation of various spin states

$$\widehat{\rho}(t) = \widehat{\rho}_{0} + \frac{(it)}{1!} [\widehat{\rho}_{0}, \widehat{\mathcal{H}}] + \frac{(it)^{2}}{2!} [\widehat{\rho}_{0}, \widehat{\mathcal{H}}], \widehat{\mathcal{H}}] + \frac{(it)^{3}}{3!} [\widehat{\rho}_{0}, \widehat{\mathcal{H}}], \widehat{\mathcal{H}}], \widehat{\mathcal{H}}]$$

$$+ \frac{(it)^{4}}{4!} [\widehat{\rho}_{0}, \widehat{\mathcal{H}}], \widehat{\mathcal{H}}], \widehat{\mathcal{H}}], \widehat{\mathcal{H}}] + \cdots$$

$$= \widehat{\rho}_{0} + it [\widehat{\rho}_{0}, \widehat{\mathcal{H}}] + \frac{it^{2}}{2!} [\widehat{\rho}, \widehat{\mathcal{H}}] + \frac{it^{3}}{3!} [\widehat{\rho}, \widehat{\mathcal{H}}] + \frac{it^{4}}{4!} [\widehat{\rho}, \widehat{\mathcal{H}}] + \cdots$$

$$(6)$$

The initial state for this system consists of singlet order on the hydride nuclei and thermal polarization on the target nucleus to give the initial density matrix in Eq. 1. For example, starting with the first derivative term in the series,  $(it [\hat{\rho}_0, \widehat{\mathcal{H}}])$ ,  $\hat{\rho}_o$  commutes with everything except the  $J_{\text{HL}}$  term in the Hamiltonian, giving

$$\dot{\rho}t = it [\hat{\rho}_{o}, \hat{H}] = it [\hat{I}_{1} \cdot \hat{I}_{2}, 2\pi J_{HL} \hat{I}_{1} \cdot \hat{L}] 
= 2\pi J_{HL} t (-\hat{I}_{1z} \hat{I}_{2x} \hat{L}_{y} + \hat{I}_{1y} \hat{I}_{2x} \hat{L}_{z} + \hat{I}_{1z} \hat{I}_{2y} \hat{L}_{x} 
-\hat{I}_{1x} \hat{I}_{2y} \hat{L}_{z} - \hat{I}_{1y} \hat{I}_{2z} \hat{L}_{x} + \hat{I}_{1x} \hat{I}_{2z} \hat{L}_{y})$$
(7)

Creation of  $\hat{L}_z$  order from Eq. 1, using the Hamiltonian in Eq. 3 and the expansion in Eq. 6, can easily be shown to require at least four commutators. Commutation of a bilinear operator with any n-spin direct product operator always adds or subtracts one spin, so the first derivative in Eq. 7 will require two more commutators with bilinear operators to transform the initial spin order into  $\hat{L}_z$ . One of those must be from the  $J_{\rm HH}$  terms, as it is the only bilinear operator with spin 2, and one must be from  $J_{\rm HL}$ . In addition, only the Zeeman term  $\Delta \omega_{\rm HL}$  distinguishes between spin up and spin down (by symmetry, no magnetization is ever formed at  $B=0~\mu{\rm T}$ ), and this term must be involved in the commutator pathway as well. Thus, the functional dependence of the leading term must be  $J_{\rm HL}^2(\Delta\,\omega_{\rm HL})J_{\rm HH}$  in the fourth derivative, leading to magnetization buildup initially proportional to  $t^4$ . A full evaluation (in the Supplementary Materials) shows

$$\ddot{p} \frac{t^4}{4!} = \frac{(it)^4}{4!} [[[[\hat{p}_0, \widehat{\mathcal{H}}], \widehat{\mathcal{H}}], \widehat{\mathcal{H}}], \widehat{\mathcal{H}}]}{4!} = (2\pi)^3 J_{\text{HL}}^2 (\Delta \omega_{\text{HL}}) J_{\text{HH}} \frac{t^4}{4!} (2\hat{L}_z - 2\hat{I}_z) + \dots$$
(8)

The  $J_{\rm HL}$  term [specifically, the nonsecular component of the  $J_{\rm HL}$  term ( $\hat{I}_{1x}\hat{L}_x+\hat{I}_{1y}\hat{L}_y$ )] is needed in the first and fourth commutators. The  $J_{\rm HH}$  and  $\Delta\omega_{\rm HL}$  terms are needed for the second and third commutators, but the order is unimportant, as the terms commute with each other. Figure 6 illustrates the "flow" into operator space in terms of the three critical spin interactions, where each arrow represents a commutation with a specified term in the Hamiltonian and successive nodes represent higher-order terms in the Taylor series expansion. The goal is to maximize the two pathways that create magnetization while minimizing the off-target pathways.

This approach helps explain the notable deviations from the LAC condition for high and low exchange rates shown in Figs. 4 and 5. In the rapid exchange limit, the achievable magnetization per unit time is expected to scale as  $k^{-3}$ , because doubling k (halving the

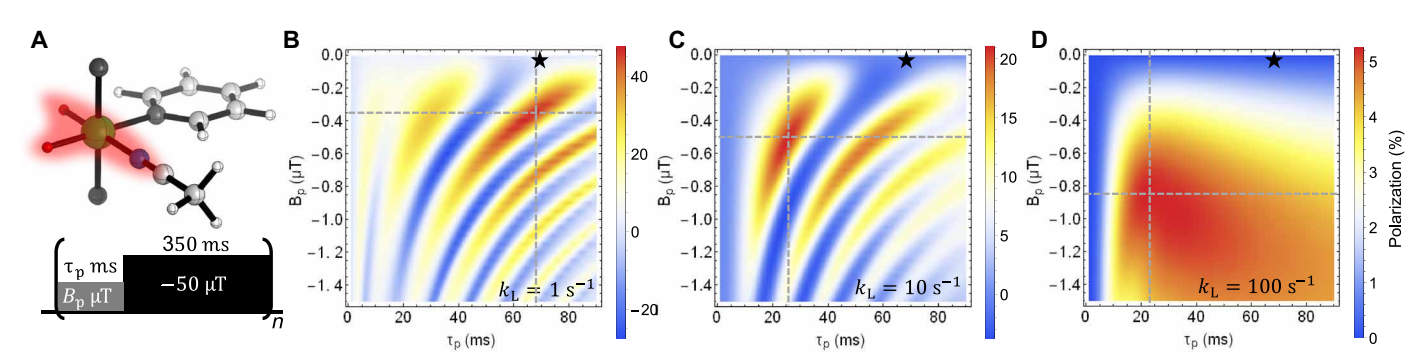


**Fig. 5. Discrepancies between optimal polarization transfer fields and LAC matching conditions in coherently pumped SABRE-SHEATH experiments. (A)** Truncated AA'X spin system with incorporated spins highlighted in red and the pulse sequence used in the simulations. **(B)** Polarization after application of the pulse sequence in (A) for 30 s under a variety of evolution field conditions  $B_p$  and durations  $\tau_p$  and  $k_L = 1$  s<sup>-1</sup>, **(C)**  $k_L = 10$  s<sup>-1</sup>, and **(D)**  $k_L = 100$  s<sup>-1</sup>. Dashed gray lines indicate maximum polarization conditions. Additional parameters: [catalyst]: [ligand] = 1:5 and  $k_H = 1$  s<sup>-1</sup>. The stars show the optimal pulse length and field predicted by a LAC calculation.

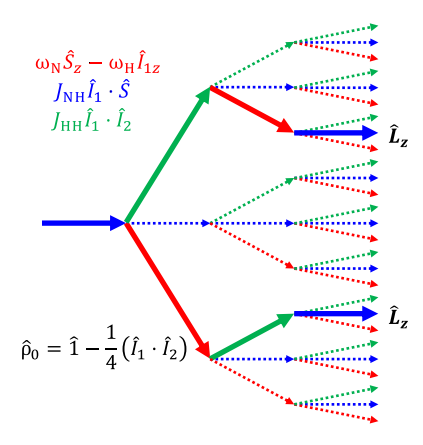


**Fig. 6. Coherence transfer pathway representation.** Demonstration of coherence pathways generated from evolution of the initial SABRE density matrix,  $\hat{\rho}_0$ , under each of the terms in the nuclear spin Hamiltonian. The polarization transfer pathway is highlighted in bold, and off-target pathways are shown with dashed lines.

lifetime of the complex) reduces the term in Eq. 8 by 16 but gives twice as many molecules, which can be (partially) polarized per unit time. In this case, higher values of the applied field (to achieve an appropriate phase shift over the complex lifetime) are strongly favored, which is again consistent with Figs. 4 and 5.

In the limit of low exchange, the optimal strategy is to maximize the ligand magnetization at around the average exchange time. The applied magnetic field is best understood as generating a phase shift; for example, as shown in the Supplementary Materials, it converts terms such as  $\hat{I}_{1x}\hat{L}_x$  into  $\hat{I}_{1x}\hat{L}_y$ , which can be converted into  $\hat{L}_z$  by the  $J_{\rm HL}$  coupling. The optimal way to do this, without overpumping other operators, is to force this term produce about  $\pi/2$  of phase shift over the lifetime of the complex. This implies that the optimum field is strongly dependent on the exchange rate.

The significance of this rotation can be seen in Fig. 7, which explicitly shows the effect of varying  $\Delta\omega_{HL}$  for a zero-field, high-field sequence (here and in all figures except Figs. 4 and 5, we include all the spins in the hydride and the ligand). With the pulse sequence in Fig. 7A, the spin system evolves under  $\hat{I}_x \hat{L}_x + \hat{I}_y \hat{L}_y$  during the zerofield pulse and then acquires some phase shift  $\theta$  under the  $\Delta\omega_{NH}$ term during the high-field pulse. In this calculation, the exchange rate is 20 s<sup>-1</sup>, giving a mean lifetime [ln  $(2)/k_L$ ] before exchange of ~35 ms. When  $\tau_p = 3$  ms as in the blue curve in Fig. 7B, the zero-field/ high-field alternation is seen about 10 times by the average complex, and efficient transfer is done with a small phase increment in each cycle (hence, the maxima occur with small deviation from  $2\pi n$ ). This also explains why the pulse sequence explored in Fig. 3 showed such sharp features at small rotations away from integral numbers of cycles about  $\Delta\omega_{HL}$ ; for the short  $\tau_d$  and  $\tau_p$  values shown there, the complex sees many pulse repetitions during its lifetime. In contrast, when  $\tau_p = 50$  ms in Fig. 7, most of the complexes see (at best) a single high-field pulse, the process is much less efficient, and a single pulse needs to produce a substantial phase shift.

We may further understand the nonintuitive dynamics presented here using average Hamiltonian theory. For the Hamiltonian in Eq. (3), using the resonance frequency difference to create a toggling frame gives

$$\widetilde{\mathcal{H}}'(t) = U\widehat{\mathcal{H}}'(t) U^{\dagger}; U(t) = \exp\left(-i\widehat{\mathcal{L}}_z \int_0^t \Delta \omega_{\mathrm{HL}}(t') dt'\right)$$

$$\widetilde{\mathcal{H}}'(t) = 2\pi J_{\text{HH}} \hat{I}_1 \cdot \hat{I}_2 + 2\pi J_{\text{HL}} \hat{I}_{1z} \hat{\mathcal{L}}_z + 2\pi J_{\text{HL}} (M(t)) (\hat{I}_{1x} \hat{\mathcal{L}}_x + \hat{I}_{1y} \hat{\mathcal{L}}_y) + N(t) (\hat{I}_{1y} \hat{\mathcal{L}}_x - \hat{I}_{1x} \hat{\mathcal{L}}_y))$$
(9)

where  $M(t) = \cos(\int_0^t \Delta \omega_{\rm HL}(t') dt')$  and  $N(t) = \sin(\int_0^t \Delta \omega_{\rm HL}(t') dt')$ . In the constant field case (fixed  $\Delta \omega_{\rm HL}$ , duration T), the integrals are easily evaluated, and we can immediately write the average Hamiltonian (the lowest order term in the Magnus expansion) as

$$\widetilde{\mathcal{H}}^{(0)}(T) = U^{\dagger}(T) \left( \frac{1}{T} \int_{0}^{T} \widetilde{\mathcal{H}}'(t) dt \right) U(T)$$

$$= U^{\dagger}(T) \left( 2\pi J_{\text{HH}} \hat{I}_{1} \cdot \hat{I}_{2} + 2\pi J_{\text{HL}} \hat{I}_{1z} \hat{L}_{z} + 2\pi J_{\text{HL}} \left( \frac{\sin(\Delta \omega_{\text{HL}} T)}{\Delta \omega_{\text{HL}} T} (\hat{I}_{1x} \hat{L}_{x} + \hat{I}_{1y} \hat{L}_{y}) + \frac{1 - \cos(\Delta \omega_{\text{HL}} T)}{\Delta \omega_{\text{HL}} T} (\hat{I}_{1y} \hat{L}_{x} - \hat{I}_{1x} \hat{L}_{y}) \right) U(T)$$

$$(10)$$

In the most common applications of average Hamiltonian theory, the sequence is cyclic, making  $U(T) = \hat{1}$ . Here, we will not impose that restriction; in Eq. 10,  $U(T) = \exp(-i\Delta \omega_{\rm HL} T \hat{L}_z)$ . This will turn out to be important when we use two different fields in the pulse sequence. At all times, U(T) commutes with both the initial density matrix and the desired final state.

There are fundamental differences between the Hamiltonians in Eqs. 3 and 10. The most obvious of which are the reduction of the nonsecular component of the H-L coupling and the introduction of an operator of the form  $(\hat{I}_{1y}\hat{L}_x - \hat{I}_{1x}\hat{L}_y)$ . This connects the same states as the normal nonsecular term but with a  $\pi/2$  phase shift for the off-diagonal operators.

Equation 10 quantifies the extent to which a resonance frequency difference truncates the nonsecular components of the scalar coupling, and it can be used in two fundamentally different ways. One way (the dominant effect in Fig. 3) is to use this to decrease the average value of the effective coupling. For example, for the  $-22.35~\mu T$  case illustrated in Fig. 3, the coupling is nearly fully truncated during the 13.5-ms pulse, so the average coupling over the entire zero-field/high-field cycle is only about one-fifth of the normal coupling (which, as Fig. 4 shows, improves the efficiency). This also explains the asymmetry in Figs. 3 and 7 between  $2\pi n$  and  $(2n+1)\pi$  rotations: In the former case, the scalar coupling during the high-field pulse is completely truncated by Eq. 10, but it is not in the latter case, and this is more consequential for shorter values of  $\tau_{\rm p}$ .

With two nonzero fields, a different effect becomes important: The two intervals can produce different effective Hamiltonians. For example, one can adjust the rotation angles of the two blocks to produce different combinations of  $(\hat{I}_{1x}\hat{L}_x+\hat{I}_{1y}\hat{L}_y)$  and  $(\hat{I}_{1y}\hat{L}_x-\hat{I}_{1x}\hat{L}_y)$ . The combination of operators  $(\hat{I}_1\cdot\hat{I}_2)$ ,  $(\hat{I}_{1x}\hat{L}_x+\hat{I}_{1y}\hat{L}_y)$ , and  $(\hat{I}_{1y}\hat{L}_x-\hat{I}_{1x}\hat{L}_y)$  can then convert the initial density matrix into  $\hat{L}_z$  magnetization in the third commutator ( $\propto t^3$ ), rather than the fourth ( $\propto t^4$ ) as in Eq. 8. Again, the optimum occurs for rotations  $\theta \approx 2\pi$  or greater, because the overall magnitude of the residual couplings is decreased.

## Optimizing nonresonant pulse sequences for polarization transfer

In this section, we use the concepts just developed to produce optimized pulse sequences for X-SABRE polarization transfer and verify the results experimentally. We start by noting that the restriction to zero field in Fig. 3 for one of the intervals is not necessary; the structure merely shifts (Fig. 8). To test the simulations experimentally,

a SABRE experiment was prepared on solutions with 100 mM  $^{15}\text{N-acetonitrile}, 33$  mM natural abundance pyridine, and 5 mM IrIMes(COD)Cl [IMes = 1,3-bis(2,4,6-trimethylphenyl)-imidazol-2-ylidene, COD = 1,5-cyclooctadiene] in methanol-d<sub>4</sub>. The solution was bubbled with 43% parahydrogen gas to allow for the formation of the active PTC [Ir(H)<sub>2</sub>(IMes)(pyr)<sub>2</sub>( $^{15}\text{N-acetonitrile}$ )]. After 30 min of continuous bubbling at lab field (~2.6 G), the sample was transferred into a triple  $\mu$ -metal shield, with a compensating solenoid powered by a standard function generator for hyperpolarization under the various two-state SABRE pulse sequences for a total

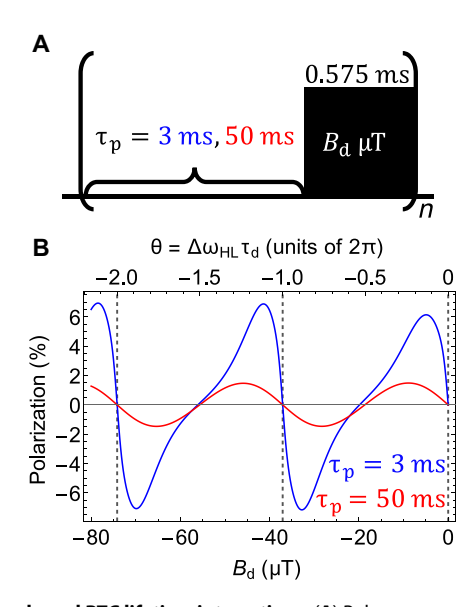


**Fig. 7. Flip angle and PTC lifetime interactions.** (**A**) Pulse sequence used in simulations. (**B**) Final polarization after application of the sequence in (A) for values of  $\tau_p = 3$  ms (blue) and  $\tau_p = 50$  ms (red) with  $B_p = 0$   $\mu$ T. Vertical dashed lines show  $2\pi n$  rotations. Simulation parameters: Ir(H)<sub>2</sub>(IMes)(pyr)<sub>2</sub>(<sup>15</sup>N-acetonitrile) spin system, [catalyst]: [ligand] = 1:20,  $k_L = 20$  s<sup>-1</sup>,  $k_H = 2$  s<sup>-1</sup>. Experiment duration: 5 s.

duration of 60 s. A slower bubbling rate was used to prevent concentration of the sample solution over many experiments. This naturally reduces the achievable polarization but preserves the consistency of experimental variables between experiments. After hyperpolarization, the sample is transferred into a 1-T  $^{15}$ N Magritek NMR for signal detection.

We varied either the high-field strength ( $-22~\mu T < B_d < 0~\mu T$ ,  $\tau_d = 2~ms$ ) or duration ( $0~ms < \tau_d < 3~ms$ ,  $B_d = -34~\mu T$ ) for the high-field pulse in a two-state SABRE sequence while maintaining a constant low field pulse ( $B_p = -0.5~\mu T$ ,  $\tau_p = 3~ms$ ). Under these conditions, we clearly see the final polarization levels in Fig. 8 oscillating at a frequency corresponding to  $\Delta\omega_{HL}$ . In agreement with the theoretical predictions, maximum positive and negative signal enhancements for this set of pulse parameters occurs at flip angles of  $\theta = 2\pi n \pm \pi/6$  with an 9% improvement in the total signal enhancement over a continuous field experiment at  $B = -0.5~\mu T$ . We demonstrate that separation of the evolution under different terms in the Hamiltonian is experimentally quite simple and improves the achievable polarization.

In the regime of Fig. 8, where  $\theta$  is relatively small compared to more optimal pulse parameters presented in this discussion and  $J_{\rm HL}$ is large, the signal enhancements are modest. More generally, it is clear from Fig. 4 that X-SABRE is fundamentally limited because  $J_{\rm HL} \gg J_{\rm HH}$ . So, a general strategy for signal enhancement uses field blocks that produce a highly reduced average coupling, as well as the desired phase shift. For example, consider the sequence in Fig. 9 below. We fix one block at a field strength  $B_d = -34 \mu T$  and duration  $\tau_d = 0.575$  ms (corresponding to a total rotation of  $\theta = -2\pi$  +  $\pi/6$ ). From equation 10, this reduces the average coupling during that period by about a factor of 7. With the lower field pulse duration fixed at  $\tau_p = 3$  ms, the field strength was swept through  $-18 \mu T$  $< B_p < 18 \,\mu\text{T}$ . Once again, there is excellent agreement between theory and experimental results. We see the predicted large sidebands with substantial signal enhancements at field strengths resulting in total rotations of  $2\pi n \pm \epsilon$  about the resonance offset term yielding a maximum enhancement of about a factor of 3.

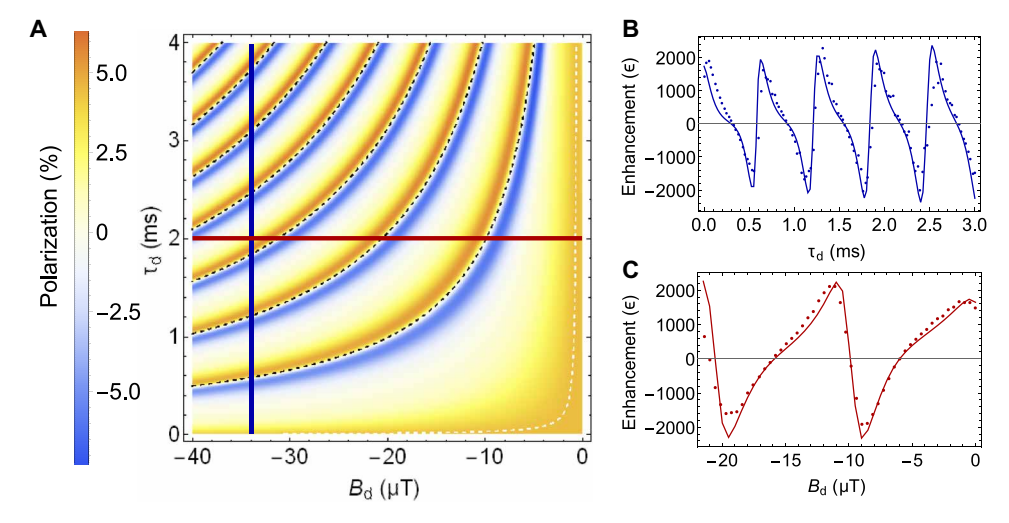


**Fig. 8. Experimental validation of theoretical predictions. (A)** Numerical simulation of polarization after a pulse sequence similar to Fig. 3 applied for 5 s, except that the zero-field portion is replaced by a field near the optimal continuous field condition. **(B)** Comparison of theoretical calculations with experimental data holding  $B_d = -34 \, \mu\text{T}$  and varying  $\tau_d$  along the blue line in (A). **(C)** Comparison of theoretical calculations with experimental data holding  $\tau_d = 2 \, \text{ms}$  and varying  $B_d$  along the red line in (A). Simulation parameters:  $k_L = 20 \, \text{s}^{-1}$ ,  $k_H = 2 \, \text{s}^{-1}$ , [catalyst]: [ligand] = 1 : 20. Simulated experiment duration: 30 s.

### Compensation for experimental inhomogeneity

The sideband resonances offer further experimental benefits in addition to increased overall polarization. The zeroes come from a lower field pulse of flip angle  $\theta \approx 2\pi n - \pi/6$ . The case n=1 corresponds to the resonance at  $6.5 \,\mu\text{T}$ . All but the near-zero field maxima and minima are offset from exact  $2\pi(n-1)$  rotations by about  $\pi/30$ . In the event of moderate inhomogeneities, which alter the applied field by some coefficient, the net flip angle for the n=1 resonance would remain almost unchanged. Two-state pulse sequences with these parameters increase the achievable polarization and are insensitive to field inhomogeneities.

On the basis of the theoretical picture presented so far, it is simple to modify sequences to compensate for inhomogeneity. Consider, for example, the zero-field/high-field sequence of Fig. 3, where substantial signal gains require very long evolution times. This pulse needs to provide a small net phase shift; so, the signal is

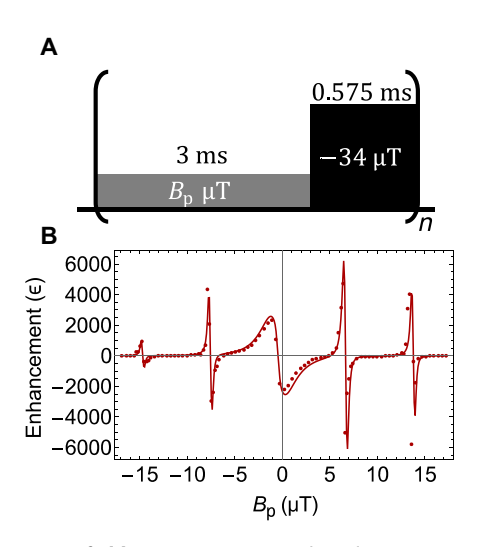


**Fig. 9. Two-state**  $B_p$  **field sweep.** Experimental results (points) compared with numerical simulation (solid line) for application of the two-field SABRE sequence shown with various lower field pulse magnitude. Simulation parameters: Ir(H)<sub>2</sub>(IMes) (pyr)<sub>2</sub>( $^{15}$ N-acetonitrile) spin system, [catalyst]: [ligand] = 1:20, and  $k_L = 20 \, \text{s}^{-1}$ .

highly sensitive to the exact amplitude (Fig. 10), and even a small amount of inhomogeneity will change this rotation enough to randomize the phase shift acquired in the evolution. However, a simple modification, replacing the long  $-22.35\,\mu\text{T}$  pulse with a slightly offset or slightly asymmetric square wave alternating between +22.35 and  $-22.35\,\mu\text{T}$ , almost completely eliminates this sensitivity. The slight asymmetry in this sequence is important. For a symmetric square wave of any amplitude, the net area is zero,  $U(T)=\hat{1}$  in Eq. 10, and the necessary phase shift does not accumulate between pulse repetitions. However, the pulse sequence in Fig. 10B has a  $\pi/2$  net rotation under the alternating high-field pulse to gain the necessary phase shift.

### DISCUSSION

Traditional SABRE polarization strategies have focused on sequences that establish resonance between spin states to pass population between states (the avoided crossing or LAC condition). The theoretical justification for this is obviously an approximation; the justification is the hope that it will give insight. However, we show here that sequences where neither the instantaneous nor average field ever approach a LAC condition can enhance polarization transfer and that the optimal field conditions vary greatly with the exchange rate. Strategic manipulation of individual terms in the Hamiltonian increases the rate of polarization transfer by favoring the interaction pathways that lead to magnetization. Because this transfer is largely dependent on the resonance frequency difference between the singlet hydrides and the target nucleus, it is possible to separately target different nuclei in the same compound, and it would be reasonable to extend this technique into larger field regimes like that of SABRE. Using a different approach to understanding the evolution of SABRE systems sequentially through multiple interactions with the Hamiltonian, we gain a deeper understanding of the system dynamics, increase the total achievable polarization for experiments, and open up the potential to selectively target different nuclei in the same ligand with a high specificity.

Our theoretical results show that in SABRE spin systems where exchange and coherent evolution occur on comparable time scales, it is more accurate to think of the resonance frequency difference as

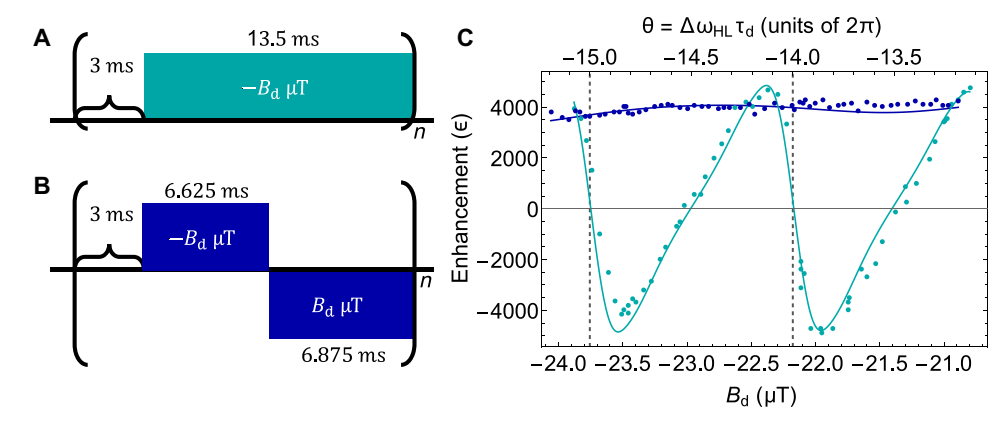


Fig. 10. Compensated and uncompensated zero-field pulse sequences. (A) Two-state pulse sequence with long higher field pulse duration ( $\tau_d = 13.5 \text{ ms}$ ) resulting in  $B_d \tau_d (\gamma_H - \gamma_N) \approx 27\pi$  to  $29\pi$  rotation across the measured fields. (B) Inhomogeneity compensated two-state pulse sequence with a bipolar higher field pulse causing a net rotation of  $\sim \pi/2$ . (C) Theoretical and experimental results for the uncompensated (cyan) and compensated (blue) two-state pulse sequences. Experiment run for 60 s on a sample composition of 5 mM Ir(IMes), 50 mM  $^{14}$ N-pyridine, and 100 mM  $^{15}$ N-acetonitrile in CD<sub>3</sub>OD. Simulation parameters: Ir(H)<sub>2</sub>(IMes)(pyr)<sub>2</sub>( $^{15}$ N-acetonitrile) spin system, [catalyst]: [ligand] = 1 : 20,  $k_L = 20 \text{ s}^{-1}$ ,  $k_H = 2 \text{ s}^{-1}$ . Simulated experiment duration: 15 s.

generating phase shifts rather than bringing spin states to an avoided crossing. The structural features in Figs. 3 and 7, for example, have no relationship to frequency matching, but phase matching in the evolution is central. While this is most clearly demonstrated in a two-state SARBE, it applies more generally to SABRE variants where chemical exchange occurs on the same time scale as the coherent dynamics. Thus, for most practical X-SABRE experiments, it is useful to go to much larger magnetic fields than the LAC conditions predict; you want a substantial phase shift during the complex lifetime. The proposed sequences presented here, while validated on a heteronuclear target, would demonstrate similar behavior in H-SABRE. However, the pulse sequence manipulations that we propose are certainly easier for X-SABRE, where rapid magnetic field shifts are trivial and the ligand hydride coupling is larger than its optimum. Two papers on similar field manipulations were submitted shortly after this work (42, 43).

The apparatus that we use here is designed to have extremely good field homogeneity; however, as shown in Fig. 10, that is not necessary with compensated sequences, which would allow for the use of larger samples where inhomogeneities would be more prevalent. We believe that the optimal strategy is to create polarization on the ligand only over a time comparable to the ligand lifetime. Within those constraints, many sequences are possible by the guidelines presented here. For example, sequences that omit the zero-field time and simply use a slightly asymmetric square wave timed to reduce J<sub>HL</sub> perform about as well; they have another potential advantage, in that  $T_1$  relaxation times are generally longer at tens of microtesla than they are at extremely low fields (44). It is completely trivial experimentally to generate arbitrary waveforms on these time scales and with these field strengths. The basic approach presented here opens up a wide range of sequences that promise to improve both the generality and effectiveness of SABRE, thus enabling new applications.

Last, while the analysis presented here has focused on applications to magnetic resonance, the assumption that avoided crossings correspond to maximum population transfer can be found more generally in other forms of spectroscopy. Such an assumption is often justifiable if conditions are coherently swept through a crossing (as in adiabatic passage); however, it is otherwise not obvious that such crossings produce optimal excitation. For instance, we find large discrepancies between the resonance conditions predicted to excite vibrational coherences in anharmonic systems (see the Supplementary Materials) (45).

### **MATERIALS AND METHODS**

### Liquid nitrogen parahydrogen generator

Parahydrogen gas was generated by passing standard dihydrogen through copper tubing containing paramagnetic impurities (FeO) and submerged in liquid nitrogen (77 K). Polytetrafluoroethylene (PTFE) tubing was used to direct flow of parahydrogen from the *p*-H<sub>2</sub> generating coil through the "inlet" tubing to a capillary tube submerged in the SABRE solution and then out to a needle valve, which regulates gas flow through an "outlet" line to the chemical hood. The full circuit is pressurized to 120 psi with a small (<1 psi) pressure differential across the NMR tube to facilitate bubbling of parahydrogen through the system. A large bore PTFE tube with an interrupting quarter turn valve connects the inlet and outlet to form a "short" valve, which diverts gas flow around the capillary tubing in

solution. When the valve is closed, parahydrogen is directed through the solution, and when the valve is open, parahydrogen flow is directed away from solution. This short valve is used to toggle parahydrogen bubbling on and off at a fixed bubbling rate, which can be set by the needle valve on the outlet gas line.

### **Preparation of SABRE sample**

A solution was prepared with 100 mM  $^{15}$ N-acetonitrile, 33 mM natural abundance pyridine, and 5 mM Ir(IMes)(COD)Cl in 500  $\mu$ l of methanol-d<sub>4</sub>. The solution was placed in a high-pressure NMR tube, which was then bubbled with 43% parahydrogen for 30 to 60 min at a lab field (~2.6 G). This period facilitates activation of the catalyst precursor [Ir(IMes)(COD)Cl] via hydrogenation of the COD ligand to generate the active form of the PTC [Ir(H)<sub>2</sub>(IMes) (pyr)<sub>2</sub>( $^{15}$ N-acetonitrile)].

### SABRE hyperpolarization procedure

The sample is transferred into a μ-metal shield (MuMETAL Zero Gauss Chambers; product ZG-206, Magnetic Shield Corporation) with a compensating solenoid for application of specified magnetic fields and field sequences (N = 184,  $\ell$  = 54.5 cm, and rise time  $\sim$ 1.5 µs). While the sample is in the shield, parahydrogen bubbling is turned on, and the field sequence of choice is applied using a BK Precision 4053 10-MHz arbitrary waveform generator. The parahydrogen gas is not saturated with methanol to prevent vaporization of the volatile solvent, so the bubbling rate was set to be low (<<60 standard cubic centimeter per minute) using the needle valve on the outlet line so as to preserve the concentration of the solution over each parameter sweep, which require 60 to 80 experiments each. One consequence of this is a reduction in the overall polarization achieved, but with the benefit of retaining consistency between experiments for purposes of accurate relative comparison. After 60 s, a switch in the circuit driving the solenoid is used to change the voltage source to a GW Instek GPS-3030D laboratory dc power supply outputting 5 V across the circuit to abruptly apply a large  $(-40 \,\mu\text{T})$  magnetic field in the same direction as the z field of the lab space to prevent adiabatic passage through the resonance conditions and resultant polarization transfer outside of the scope of the experimental conditions. Then, the sample is removed from the shield and compensating solenoid and manually transferred to a 1-T 15N Magritek NMR for signal detection. All experiments in this work were performed at 20°C.

### Application of field sequences

For continuous field experiments, the arbitrary waveform generator (AWG) is set to apply a triggered pulse lasting 75 s at a chosen voltage. The sample is placed in the  $\mu\text{-metal}$  shield, the pulse is triggered, and then the parahydrogen bubbling is turned on. After 60 s, the applied field is switched to be continuous with the lab field and transferred to the NMR for detection. The applied voltage was swept with the intention of identifying two critical points: the maximum achievable enhancement under a continuous field experiment and the voltage needed to generate a compensating field to oppose the residual field in the shield to generate a  $0\text{-}\mu\text{T}$  condition in the shield.

For uncompensated field sequences, the AWG is set to output a repeating pulse sequence with two alternating voltages  $V_p$  and  $V_d$  for durations  $\tau_p$  and  $\tau_d$ . The sequence is left on, and parahydrogen is bubbled for a 60-s experiment. For compensated field sequences, the waveforms shown in the Supplementary Materials were loaded

into the AWG and applied for 60 s with bubbling. Additional discussion of the application of these pulse sequences is available in the Supplementary Materials.

### **SUPPLEMENTARY MATERIALS**

Supplementary material for this article is available at https://science.org/doi/10.1126/sciadv.abl3708

### **REFERENCES AND NOTES**

- J. H. Ardenkjær-Larsen, B. Fridlund, A. Gram, G. Hansson, L. Hansson, M. H. Lerche, R. Servin, M. Thaning, K. Golman, Increase in signal-to-noise ratio of > 10,000 times in liquid-state NMR. *Proc. Natl. Acad. Sci.* 100, 10158–10163 (2003).
- T. G. Walker, W. Happer, Spin-exchange optical pumping of noble-gas nuclei. Rev. Mod. Phys. 69, 629–642 (1997).
- R. W. Adams, J. A. Aguilar, K. D. Atkinson, M. J. Cowley, P. I. P. Elliott, S. B. Duckett, G. G. R. Green, I. G. Khazal, J. López-Serrano, D. C. Williamson, Reversible interactions with para-hydrogen enhance NMR sensitivity by polarization transfer. Science 323, 1708–1711 (2009).
- K. D. Atkinson, M. J. Cowley, P. I. P. Elliott, S. B. Duckett, G. G. R. Green, J. López-Serrano, A. C. Whitwood, Spontaneous transfer of Parahydrogen derived spin order to pyridine at low magnetic field. J. Am. Chem. Soc. 131, 13362–13368 (2009).
- A. N. Pravdivtsev, A. V. Yurkovskaya, H. M. Vieth, K. L. Ivanov, R. Kaptein, Level anti-crossings are a key factor for understanding para-hydrogen-induced hyperpolarization in SABRE Experiments. ChemPhysChem 14, 3327–3331 (2013).
- T. Theis, M. L. Truong, A. M. Coffey, R. V. Shchepin, K. W. Waddell, F. Shi, B. M. Goodson, W. S. Warren, E. Y. Chekmenev, Microtesla SABRE enables 10% nitrogen-15 nuclear spin polarization. *J. Am. Chem. Soc.* 137, 1404–1407 (2015).
- M. L. Truong, T. Theis, A. M. Coffey, R. V. Shchepin, K. W. Waddell, F. Shi, B. M. Goodson, W. S. Warren, E. Y. Chekmenev, 15N hyperpolarization by reversible exchange using SABRE-SHEATH. J. Phys. Chem. C 119, 8786–8797 (2015).
- T. Theis, M. Truong, A. M. Coffey, E. Y. Chekmenev, W. S. Warren, LIGHT-SABRE enables efficient in-magnet catalytic hyperpolarization. *J. Magn. Reson.* 248, 23–26 (2014).
- S. Knecht, A. S. Kiryutin, A. V. Yurkovskaya, K. L. Ivanov, Efficient conversion of anti-phase spin order of protons into 15N magnetisation using SLIC-SABRE. *Mol. Phys.* 117, 2762–2771 (2019).
- A. N. Pravdivtsev, A. V. Yurkovskaya, H.-M. Vieth, K. L. Ivanov, Spin mixing at level anti-crossings in the rotating frame makes high-field SABRE feasible. *Phys. Chem. Chem. Phys.* 16. 24672–24675 (2014).
- S. S. Roy, G. Stevanato, P. J. Rayner, S. B. Duckett, Direct enhancement of nitrogen-15 targets at high-field by fast ADAPT-SABRE. J. Magn. Reson. 285, 55–60 (2017).
- J. R. Lindale, S. L. Eriksson, C. P. N. Tanner, Z. Zhou, J. F. P. Colell, G. Zhang, J. Bae, E. Y. Chekmenev, T. Theis, W. S. Warren, Unveiling coherently driven hyperpolarization dynamics in signal amplification by reversible exchange. *Nat. Commun.* 10, 395 (2019).
- J. R. Lindale, C. P. Tanner, S. L. Eriksson, W. S. Warren, Decoupled LIGHT-SABRE variants allow hyperpolarization of asymmetric SABRE systems at an arbitrary field. *J. Magn. Reson.* 307, 106577 (2019).
- D. A. Barskiy, S. Knecht, A. V. Yurkovskaya, K. L. Ivanov, SABRE: Chemical kinetics and spin dynamics of the formation of hyperpolarization. *Prog. Nucl. Magn. Reson. Spectrosc.* 114-115, 33–70 (2019).
- M. J. Cowley, R. W. Adams, K. D. Atkinson, M. C. R. Cockett, S. B. Duckett, G. G. R. Green, J. A. B. Lohman, R. Kerssebaum, D. Kilgour, R. E. Mewis, Iridium N-heterocyclic carbene complexes as efficient catalysts for magnetization transfer from para-hydrogen. *J. Am. Chem. Soc.* 133, 6134–6137 (2011).
- B. J. A. van Weerdenburg, S. Glöggler, N. Eshuis, A. H. J. Engwerda, J. M. M. Smits, R. de Gelder, S. Appelt, S. S. Wymenga, M. Tessari, M. C. Feiters, B. Blümich, F. P. J. T. Rutjes, Ligand effects of NHC-iridium catalysts for signal amplification by reversible exchange (SABRE). Chem. Commun. 49, 7388–7390 (2013).
- J. R. Lindale, S. L. Eriksson, C. P. Tanner, W. S. Warren, Infinite-order perturbative treatment for quantum evolution with exchange. Sci. Adv. 6, eabb6874 (2020).
- N. Eshuis, N. Hermkens, B. J. A. van Weerdenburg, M. C. Feiters, F. P. J. T. Rutjes,
   S. S. Wijmenga, M. Tessari, Toward nanomolar detection by NMR through SABRE hyperpolarization. J. Am. Chem. Soc. 136, 2695–2698 (2014).
- K. L. Ivanov, A. N. Pravdivtsev, A. V. Yurkovskaya, H.-M. Vieth, R. Kaptein, The role of level anti-crossings in nuclear spin hyperpolarization. *Prog. Nucl. Magn. Reson. Spectrosc.* 81, 1–36 (2014).
- B. A. Rodin, K. L. Ivanov, Representation of population exchange at level anti-crossings. Magn. Reson. 1, 347–365 (2020).
- F. Colegrove, P. Franken, R. Lewis, R. Sands, Novel method of spectroscopy with applications to precision fine structure measurements. *Phys. Rev. Lett.* 3, 420–422 (1959).

- 22. L. D. Landau, Zur theorie der energieubertragung ii. Z. Sowjetunion 2, 46–51 (1932).
- 23. E. Majorana, Atomi orientati in campo magnetico variabile. Il Nuovo Cimento 9, 43-50 (1932).
- E. C. Stückelberg, Theory of inelastic collisions between atoms (theory of inelastic collisions between atoms, using two simultaneous differential equations). Helv. Phys. Acta 5, 369–422 (1932)
- C. Zener, Non-adiabatic crossing of energy levels. Proc. R. Soc. Lond. Ser. A 137, 696–702 (1932).
- W. Hanle, Über magnetische beeinflussung der polarisation der resonanzfluoreszenz.
   Z. Phys. 30, 93–105 (1924).
- R. W. Wood, A. Ellett, On the influence of magnetic fields on the polarisation of resonance radiation. Proc. R. Soc. Lond. Ser. A 103, 396–403 (1923).
- N. M. Ariyasingha, J. R. Lindale, S. L. Eriksson, G. P. Clark, T. Theis, R. V. Shchepin, N. V. Chukanov, K. V. Kovtunov, I. V. Koptyug, W. S. Warren, E. Y. Chekmenev, Quasiresonance fluorine-19 signal amplification by reversible exchange. *J. Phys. Chem. lett.* 10, 4229–4236 (2019).
- M. E. Gemeinhardt, M. N. Limbach, T. R. Gebhardt, C. W. Eriksson, S. L. Eriksson,
  J. R. Lindale, E. A. Goodson, W. S. Warren, E. Y. Chekmenev, B. M. Goodson, "Direct" 13C
  hyperpolarization of 13C-acetate by microtesla NMR signal amplification by reversible
  exchange (SABRE). Angew. Chem. Int. Ed. 59, 418–423 (2020).
- M. J. Burns, P. J. Rayner, G. G. R. Green, L. A. R. Highton, R. E. Mewis, S. B. Duckett, Improving the hyperpolarization of 31P nuclei by synthetic design. *J. Phys. Chem. B* 119, 5020–5027 (2015).
- V. V. Zhivonitko, I. V. Skovpin, I. V. Koptyug, Strong 31P nuclear spin hyperpolarization produced via reversible chemical interaction with parahydrogen. *Chem. Commun.* 51, 2506–2509 (2015).
- J. F. P. Colell, A. W. J. Logan, Z. Zhou, R. V. Shchepin, D. A. Barskiy, G. X. Ortiz Jr., Q. Wang, S. J. Malcolmson, E. Y. Chekmenev, W. S. Warren, T. Theis, Generalizing, extending, and maximizing nitrogen-15 hyperpolarization induced by parahydrogen in reversible exchange. J. Phys. Chem. C 121, 6626–6634 (2017).
- R. W. Adams, S. B. Duckett, R. A. Green, D. C. Williamson, G. G. Green, A theoretical basis for spontaneous polarization transfer in non-hydrogenative parahydrogen-induced polarization. J. Chem. Phys. 131, 194505 (2009).
- D. A. Barskiy, A. N. Pravdivtsev, K. L. Ivanov, K. V. Kovtunov, I. V. Koptyug, A simple analytical model for signal amplification by reversible exchange (SABRE) process. *Phys. Chem. Phys.* 18, 89–93 (2016).
- S. Knecht, A. N. Pravdivtsev, J.-B. Hövener, A. V. Yurkovskaya, K. L. Ivanov, Quantitative description of the SABRE process: Rigorous consideration of spin dynamics and chemical exchange. RSC Adv. 6, 24470–24477 (2016).
- A. N. Pravdivtsev, J. B. Hövener, Simulating non-linear chemical and physical (CAP) dynamics of signal amplification by reversible exchange (SABRE). Chem Eur J 25, 7659–7668 (2019).
- A. S. Kiryutin, A. V. Yurkovskaya, H. Zimmermann, H. M. Vieth, K. L. Ivanov, Complete magnetic field dependence of SABRE-derived polarization. *Magn. Reson. Chem.* 56, 651–662 (2018)
- A. N. Pravdivtsev, K. L. Ivanov, A. V. Yurkovskaya, P. A. Petrov, H. H. Limbach, R. Kaptein, H. M. Vieth, Spin polarization transfer mechanisms of SABRE: A magnetic field dependent study. J. Magn. Reson. 261, 73–82 (2015).
- A. N. Pravdivtsev, I. V. Skovpin, A. I. Svyatova, N. V. Chukanov, L. M. Kovtunova,
   V. I. Bukhtiyarov, E. Y. Chekmenev, K. V. Kovtunov, I. V. Koptyug, J. B. Hövener, Chemical exchange reaction effect on polarization transfer efficiency in SLIC-SABRE. *Chem. Eur. J.* 122, 9107–9114 (2018).
- T. Theis, G. X. Ortiz Jr., A. W. J. Logan, K. E. Claytor, Y. Feng, W. P. Huhn, V. Blum, S. J. Malcolmson, E. Y. Chekmenev, Q. Wang, W. S. Warren, Direct and cost-efficient hyperpolarization of long-lived nuclear spin states on universal15N2-diazirine molecular tags. Sci. Adv. 2, e1501438 (2016).
- J. Eills, J. W. Blanchard, T. Wu, C. Bengs, J. Hollenbach, D. Budker, M. H. Levitt, Polarization transfer via field sweeping in parahydrogen-enhanced nuclear magnetic resonance. *J. Chem. Phys.* 150, 174202 (2019).
- 42. L. Dagys, C. Bengs, M. H. Levitt, Low-frequency excitation of singlet–triplet transitions. Application to nuclear hyperpolarization. *J. Chem. Phys.* **155**, 154201 (2021).
- A. N. Pravdivtsev, N. Kempf, M. Plaumann, J. Bernarding, K. Scheffler, J. B. Hövener, K. Buckenmaier, Front Cover: (ChemPhysChem 23/2021). ChemPhysChem 22, 2379–2379 (2021).
- R. V. Shchepin, L. Jaigirdar, E. Y. Chekmenev, Spin–lattice relaxation of hyperpolarized metronidazole in signal amplification by reversible exchange in micro-tesla fields. *J. Phys. Chem. C* 122, 4984–4996 (2018).
- J. P. Dahl, M. Springborg, The Morse oscillator in position space, momentum space, and phase space. J. Chem. Phys. 88, 4535–4547 (1988).
- C. P. N. Tanner, J. R. Lindale, S. L. Eriksson, Z. Zhou, J. F. P. Colell, T. Theis, W. S. Warren, Selective hyperpolarization of heteronuclear singlet states via pulsed microtesla SABRE. J. Chem. Phys. 151, 044201 (2019).

### Acknowledgments

**Funding:** This work was supported by the National Science Foundation under grant CHE-2003109. **Author contributions:** Conceptualization: S.L.E., W.S.W., J.R.L., and X.L. Methodology: S.L.E. Software: S.L.E. Investigation: S.L.E. Visualization: S.L.E. and W.S.W. Supervision: W.S.W. Writing (original draft): W.S.W. and S.L.E. Writing (review and editing): W.S.W., S.L.E., and J.R.L. **Competing interests:** The authors declare that they have no competing interests. **Data and materials availability:** All data needed to evaluate the

conclusions in the paper are present in the paper and/or the Supplementary Materials. Raw data are available at the Duke Research Data Repository (https://doi.org/10.7924/r4dr2z58t).

Submitted 9 July 2021 Accepted 24 January 2022 Published 16 March 2022 10.1126/sciadv.abl3708

# Downloaded from https://www.science.org at Duke University on June 15, 2022

# **Science** Advances

# Improving SABRE hyperpolarization with highly nonintuitive pulse sequences: Moving beyond avoided crossings to describe dynamics

Shannon L. ErikssonJacob R. LindaleXiaoqing LiWarren S. Warren

Sci. Adv., 8 (11), eabl3708. • DOI: 10.1126/sciadv.abl3708

View the article online

https://www.science.org/doi/10.1126/sciadv.abl3708

**Permissions** 

https://www.science.org/help/reprints-and-permissions

to original U.S. Government Works. Distributed under a Creative Commons Attribution NonCommercial License 4.0 (CC BY-NC).